https://doi.org/10.20965/jdr.2017.p0646

Paper:

Machine Learning Based Building Damage Mapping from the ALOS-2/PALSAR-2 SAR Imagery: Case Study of 2016 Kumamoto Earthquake

Yanbing Bai[*,†], **Bruno Adriano**[**], **Erick Mas**[**] **and Shunichi Koshimura**[**]

[*]Graduate School of Engineering, Tohoku University
6-6-4 Aramaki-Aza Aoba, Aob-ku, Senda, Miyagi 980-8579, Japan
[†]Corresponding author, E-mail: bai.yanbing.q3@dc.tohoku.ac.jp
[**]International Research Institute of Disaster Science, Tohoku University, Miyagi, Japan
[Received December 28, 2016; accepted June 20, 2017]

Synthetic Aperture Radar (SAR) remote sensing is a useful tool for mapping earthquake-induced building damage. A series of operational methodologies based on SAR data using either multi-temporal or only post-event SAR images have been developed and used to serve disaster activities. This presents a critical problem: which method is more likely to obtain reliable results and should be adopted for disaster response when both pre- and post-event SAR data are available? To explore this question, this study takes the 2016 Kumamoto earthquake as a case study. ALOS-2/PALSAR-2 SAR images were employed with a machine learning framework to quantitatively compare the performance of building damage mapping using only post-event SAR images and mapping using multi-temporal SAR images. The results show that an overall accuracy of 64.5% was achieved when only post-event SAR images were used, which is 2.3% higher than the overall accuracy when multi-temporal SAR images were used. The estimated building damage ratio for the former and the latter are 29.7% and 31.1%, respectively, which are both close to the building damage ratio obtained from an optical image.

Keywords: 2016 Kumamoto earthquake, building damage mapping, ALOS-2/PALSAR-2, synthetic aperture radar, machine learning

1. Introduction

Synthetic Aperture Radar remote sensing technology has been widely acknowledged as a useful tool for monitoring earthquake disasters, and the advantages of using this approach to recent earthquakes have been spotlighted [1, 2]. SAR images can be employed as alternative ground truth data to capture damage information to construct a near real-time earthquake-induced building damage map [3]. The superiority of remote sensing for earthquake disaster monitoring lies in its large-scale rapid observation. Its necessity has been highlighted for disasters occurring in inaccessible areas [4].

In general, there are two methodologies for detecting building damage from SAR images. The first and most widely used is the multi-temporal SAR image-based change detection technique, the basic principle of which is that radar echo is sensitive to the changes in man-made scatterers. Thus, if buildings are damaged, these changes can be detected from the multi-temporal SAR image. Changes in the radar backscattering coefficient have been widely used for mapping building damage from earthquakes [5–12]. The changes are usually quantified by calculating the difference or ratio between the backscattering coefficients of multi-temporal acquisitions [13]. Guida et al. (2010) employed the double reflection feature extracted from multi-temporal COSMO-SkyMed images to detect destroyed buildings in the 2009 L'Aquila earthquake [14]. Chen et al. (2012) used the ratio of double bounce scattering from a fully polarimetric ALOS/PALSAR image to estimate the urban damage in the 2011 Tohoku earthquake [15]. Coherence has also been used to map the urban damage induced by the Bam earthquake [16, 17] and by Watanabe et al. (2016) to monitor urban damage from the 2015 Nepal earthquake [18]. In addition, Yun et al. (2016) have developed a coherence-based automatic building damage mapping method and successfully applied it to the 2015 Nepal earthquake [1].

Although the change detection method is effective for detecting building damage, it presents a formidable challenge when pre-event SAR archives are not available. For such circumstances, a classification methodology using only post-event fully polarimetric SAR imagery was proposed and applied to mapping earthquake-induced building damage [19, 20]. In order to extend this classification methodology to more extensive SAR data types, such as single polarization SAR datasets, a machine learning-based building damage mapping (MLBDM) technique was introduced and was demonstrated to be powerful for distinguishing buildings damaged by an earthquake from sub-meter Very High Resolution (VHR) SAR imagery [21, 22]. Nevertheless, two questions still need to be resolved in regard to the MLBDM methodology: 1) the MLBDM methodology has solely been used to perform building damage mapping in block scale [36] or us-

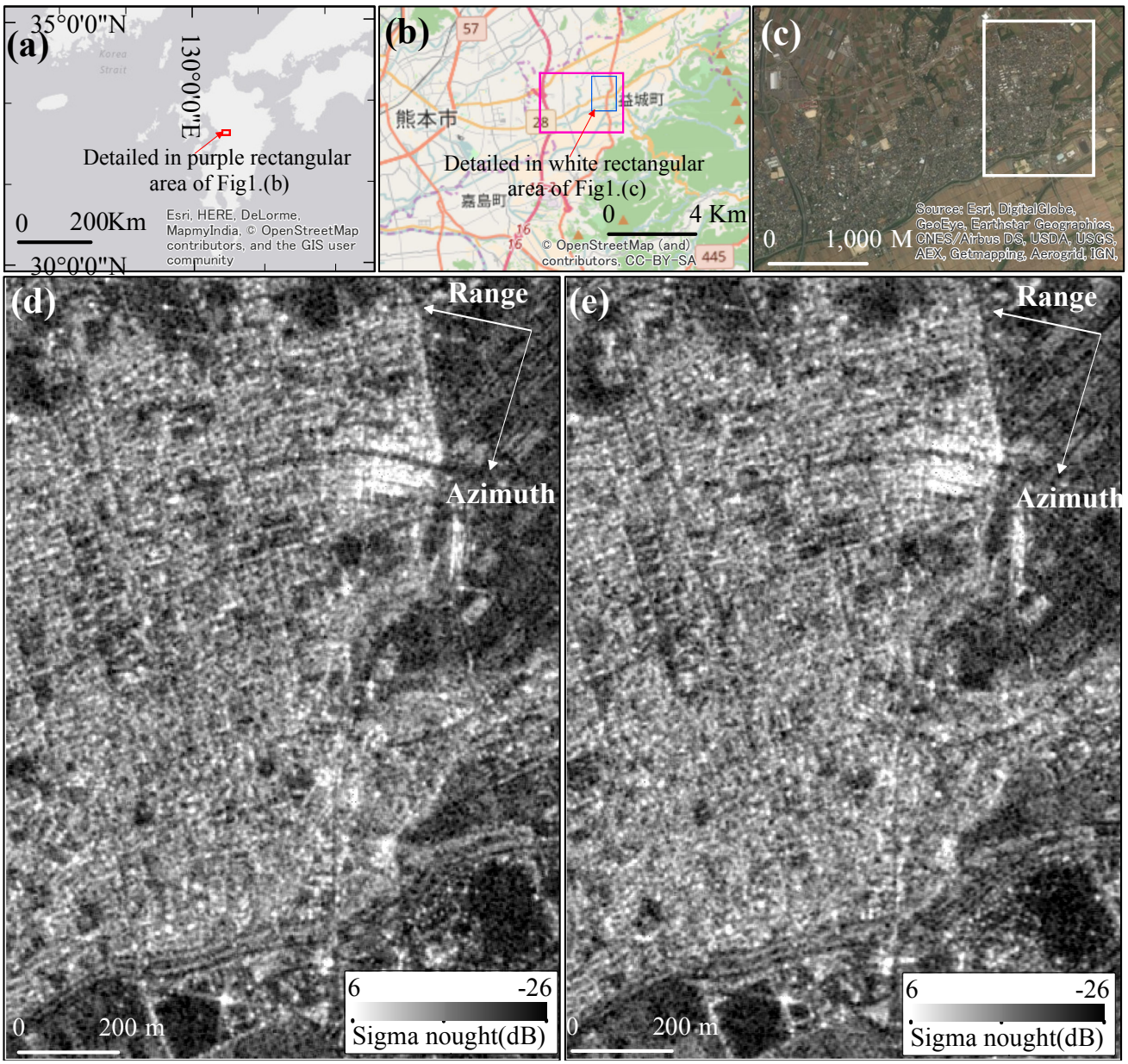

Fig. 1. Study area and ALOS-2/PALSAR-2 data used in this study: (a) location of Kumamoto city; (b) more detailed map of Kumamoto city; Mashiki town is located in the northeast of Kumamoto city; (c) optical imagery of Mashiki town; our study area is located in the northeast of Mashiki town in the white rectangular area; (d) pre-event and (e) post-event ALOS-2/PALSAR-2 data from the study area.

ing VHR airborne SAR; that is, the applicability of the MLBDM methodology to space-borne SAR imagery has not yet been reported; 2) the MLBDM methodology has only been used on the features in post-event SAR imagery; its performance when using multi-temporal SAR image features has not yet been reported.

The objective of this study is therefore to test its performance of building damage mapping when using space-borne SAR imagery and to establish whether the employment of multi-temporal SAR image features in the MLBDM methodology can improve its performance of damage mapping.

2. Study Area and Datasets

2.1. Mashiki Town District

The study area is located in Kumamoto Prefecture, Kyushu region in Japan as shown in **Fig. 1(a)**. The specific area is the town of Mashiki, which is located in the northeast of Kumamoto city as shown by the blue rectangular area in **Fig. 1(b)**. Greater detail of our study area is shown in white rectangular area in **Fig. 1(c)**. This area was hit hardest during the April 16th Mw7.0 mainshock of the 2016 Kumamoto, Japan, earthquake, and in this area, the ratio of totally collapsed wooden houses reportedly reached as high as 50% [23]. The estimated population

Table 1. The description of the ALOS-2/PALSAR-2 dataset in this study.

Type	Date	Polarization	Spatial Resolution	Off-nadir angle	Path direction	Level
ALOS-2/PALSAR-2	2016/03/07	HH	2.5m	32.8°	Descending	SLC
ALOS-2/PALSAR-2	2016/04/18	HH	2.5m	32.8°	Descending	SLC

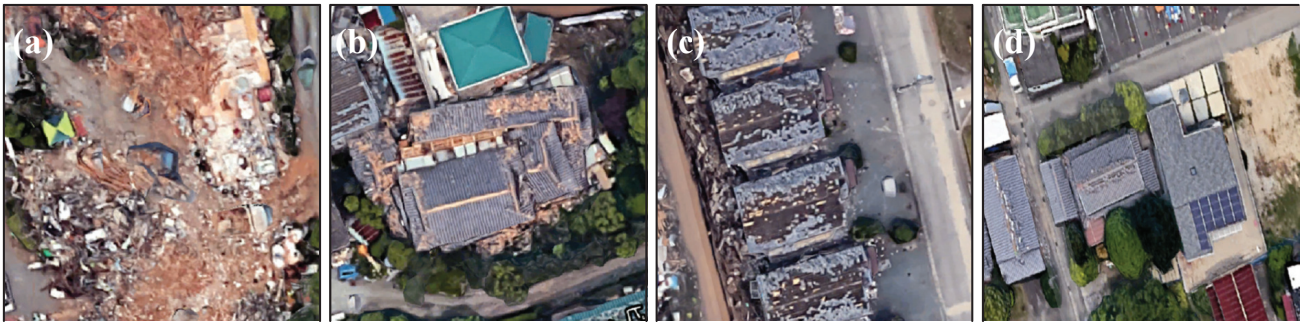

Fig. 2. Typical building damage patterns in the 2016 Kumamoto earthquake: (a) the buildings become debris; (b) the structure of buildings is severely damaged; (c) the roof tiles are severely damaged; (d) no significant damage can be observed.

of Mashiki is 326,000 with a density of 496.42 persons per km^2 as of 2003. On May 2, 2016, a reconnaissance survey was organized by Saitama University to investigate the building damage caused by the earthquake in this area. The investigation revealed that old houses suffered most of the damage, while new buildings showed almost no damage except for some shear cracks appearing on the walls.

2.2. ALOS-2/PALSAR-2 Images and Ground Truth Data

The ALOS-2 radar earth observation satellite was launched in May 2014. PALSAR-2, aboard ALOS-2, is an L-band Synthetic Aperture Radar antenna. In this study, we use a pair of multi-temporal ALOS-2/PALSAR-2 images acquired on March 7, 2016 and April 18, 2016. The images were taken by the HH polarization in the descending path. The azimuth resolution is about 2.21 m, and the ground range resolution is about 1.43 m. The off-nadir angle is 32.8°. The image was recorded as a single-look complex (SLC) product. A summary of the ALOS-2/PALSAR-2 datasets used in this study is shown in **Table 1**.

The ground truth data, shown in **Fig. 5(c)**, used in this study were visually interpreted from very high resolution optical imagery provided by Google Maps [24].

In general, four types of buildings were observed in this area: Class 1: buildings are in ruins and present debris as shown in **Fig. 2(a)**; Class 2: the structure of the buildings is severely damaged, as in vertical subsidence or collapse of the side wall shown in **Fig. 2(b)**; Class 3: the roof tiles are damaged as shown in **Fig. 2(c)**; Class 4: no significant damage can be observed as shown in **Fig. 2(d)**. Since the ground truth data was constructed from an orthographic projection of the optical image, it is very difficult to judge the internal damage of the buildings. We therefore defined those buildings with a large number of damaged tiles to be damaged buildings. Buildings in Classes 1, 2 and 3 are thus considered damaged, while those in Class 4 are categorized as undamaged.

3. Methodology

3.1. Principle

The basic principle of this methodology is the assumption that the scattering characteristics of damaged and undamaged buildings differ and are consequently distinguishable. The theoretical basis is as follows. First, the backscattering coefficient of ground scatters like buildings is a function of the radar wavelength and is closely related to the surface roughness of the scatters. In general, intact buildings present stronger backscattering due to the double bounce scattering. Collapsed buildings present relatively weaker backscattering due to reduced double bounce scattering. Second, the scattering characteristics of intact buildings demonstrate higher consistency in the distribution of the backscattering coefficient within the resolution cell due to the relatively consistent scattering type compared with the random scattering of collapsed buildings. Specifically, if the majority of tiles on a building have been severely damaged, the heterogeneity of backscattering within the roof area will decrease, and we assume that this kind of difference can be detected by statistical analysis such as the texture analysis [25]. Finally, as the high-dimensional feature-based machine learning technique is a powerful tool for classification, the differences between damaged buildings and undamaged buildings can be highlighted by integrating features related to the scattering characteristics. The data mining software WEKA (Ver. 3.6.9) was employed to implement the supervised machine learning algorithms [26]. Image

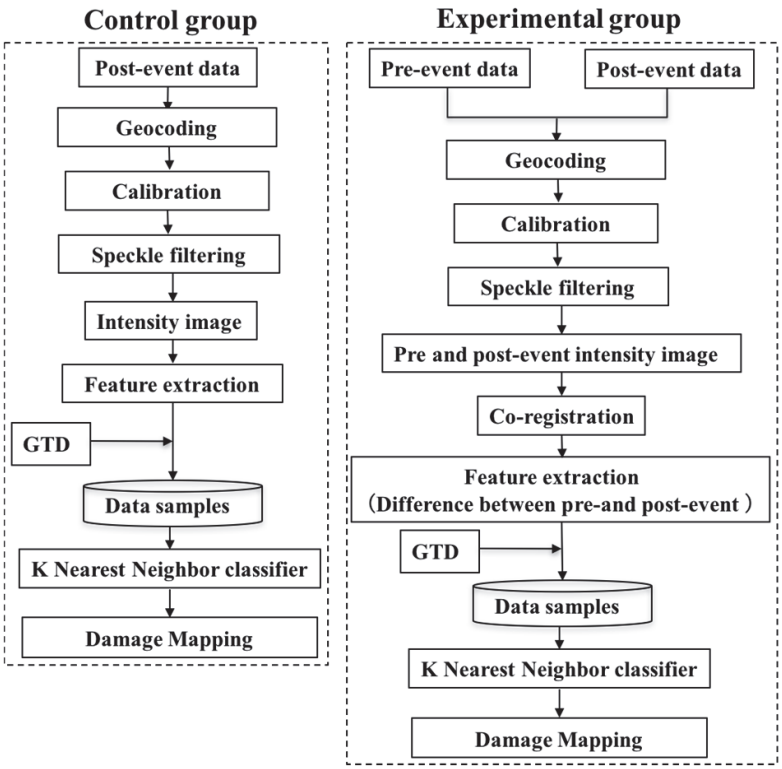

Fig. 3. Flowchart of the methodology used in this study.

processing and mapping were performed on the ArcGIS and ENVI/SARscape software [27]. A flowchart of the methodology used in this study is shown in **Fig. 3**.

3.2. Image Pre-Processing

Pre-processing of the ALOS-2/PALSAR-2 images was implemented in the ENVI/SARscape software. First, the ALOS-2/PALSAR-2 images were processed with one look for both the range and azimuth to preserve the high resolution. The images were then geocoded using the Shuttle Radar Topography Mission DEM, with a pixel resolution of around 2.5 m. Next, radiometric calibration was performed to transform the digital number into the Sigma Naught (σ) value, followed by co-registration of the pre- and post-event SAR images. Finally, the most widely used, enhanced Lee filter with a window size of 3×3 pixels was adopted to reduce the speckle noise of the SAR images. The processed pre-event and post-event SAR images are shown in **Figs. 1(d)** and **1(e)**, respectively.

3.3. Feature Extraction

In this study, the texture features derived from the SAR images are investigated. The texture features mainly reflect the statistical properties of a SAR image and could be used as features to distinguish buildings with different levels of damage [25]. The two kinds of texture features described below are employed for classification; both were extracted from the post-event and the multitemporal SAR images within individual building footprints. First, the Gray-level Histogram is a statistical histogram of the graylevel frequency within an image; the statistical properties of damaged buildings and undamaged buildings within an image are reflected in the gray-level histogram. In this paper, the features calculated from the gray-level histogram are data range, mean, variance, and skewness, all of which were investigated using window sizes of 5×5, 7×7, 9×9, and 11×11.

These features were calculated with the ENVI/SARscape software. Second, Gray-level Co-occurrence Matrices (GLCM), which were proposed by Haralick [37], are a series of secondorder statistics that reflect the frequency of different spatial combinations of gray levels between two points appearing in the image. GLCM is a matrix function of pixel distance and angle; the pixel distance is controlled by the calculation window size, and the angle is the azimuth angle of two pixels. In this paper, the features extracted from the GLCM are contrast, dissimilarity, homogeneity, mean, variance, correlation, and entropy respectively, as the directions of GLCM calculation have effect on the feature characteristics [38], therefore, in this study, each of the above mentioned 7 features were calculated in 0°, 45°, 90°, 135° respectively, in total, we have 28 GLCM features. All of these features were investigated using window sizes of 5×5, 7×7, 9×9, and 11×11. These features were calculated with the Sentinel-1 Toolbox software [28]. A summary of the features used in this study is presented in **Table 2**.

Table 2. Summary of features used in this study.

	Tested features	No.
Polarimetric	Backscattering coefficient ($\sigma_{HH}{}^{0}$)	1
Texture	$GLCM_{0°,45°,90°,135°}$ (Contrast, Dissimilarity, Homogeneity, Mean, Variance, Correlation, Entropy)	28
	GH (Data Range, Variance, Skewness, Mean)	4

3.4. Control Experiment

For the control group, all of the texture features were calculated from only the post-event SAR image. The purpose of the control group is to test the performance of building damage mapping from using only the post-event space-borne SAR image. For the experimental group, all of the polarimetric and texture features were calculated from both pre- and post-event SAR images; the differences between the pre- and post-event SAR images were calculated for each feature and were used as feature input. The purpose of the experimental group is to investigate whether using only the post-event SAR image is the optimal strategy when pre-event images are not available.

3.5. Supervised Learning for Damage Classification

All of the features were extracted for each building in the study area within the building footprint. Together with the ground truth data, they were used to train the supervised learning classifier. In the earthquake-affected area that we tested, damaged buildings account for only a small fraction of the total. This is a typical case, reflecting an imbalance between damaged and undamaged buildings, and it potentially induces a bias in the classification. Many methods have been proposed to account for such effects in the context of a variety of statistical learning methodologies [29–31]. None of the proposed approaches up to this point provides a universal advantage in all situations [32, 33]. In addition, the class imbalance between damaged and undamaged buildings in the case of earthquakes is high. To verify the accuracy of our method in practical application, we employed the imbalanced data directly to perform the analysis. In our evaluation, 10-fold cross-validation was used to assess how the results of a training model would generalize to an independent test dataset. In the 10-fold cross-validation, all of the samples were randomly, proportionally partitioned into ten equally sized subsamples. Of the ten subsamples, nine were used as training data to create the model, with the remaining subsample used as the validation data to test the model. In this way, the cross-validation process is repeated ten times; the ten results can then be averaged to produce a single estimate. In this evaluation, we tested many machine learning algorithms to predict the damage attributes of buildings. The K-Nearest Neighbors algorithm performed best and was selected as the classifier for the accuracy assessment.

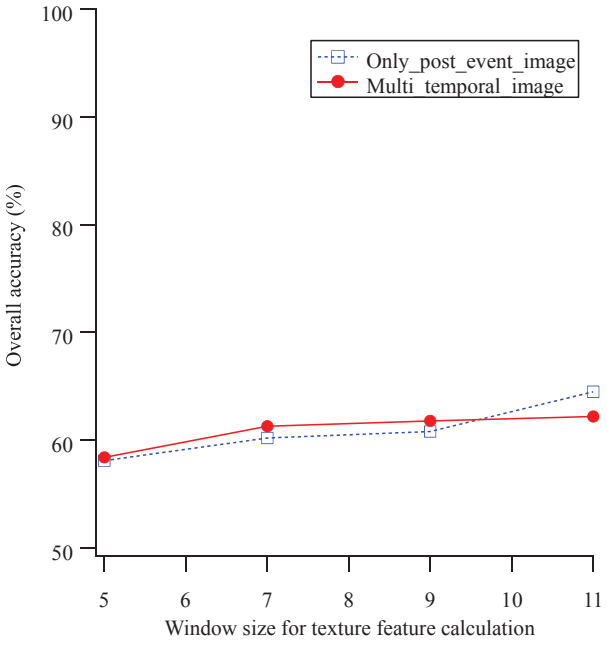

Fig. 4. Overall accuracy of building damage mapping using only the post-event SAR image and using the multi-temporal SAR image, respectively.

4. Results and Discussion

The overall classification accuracy of the control group and the experimental group for four different calculation window sizes are shown in **Fig. 4**. The results indicate that using the multi-temporal SAR image does not improve the classification accuracy, nor does it decrease the accuracy. This result suggests that the multi-temporal SAR images are not necessary for the MLBDM methodology. In addition, the overall accuracy for the control group and the experimental group increased as the calculation window size increased. This is probably because larger windows can guarantee that various sizes of buildings can be embedded in such a local boxcar. For simplicity, the 11×11 window size was adopted in this study for deep analysis. The results of damage classification in Mashiki town using only the post-event image and using the multi-temporal SAR image are shown in **Figs. 5(a)** and **5(b)**, respectively. The accuracy assessment of the two classifications is shown in **Table 3**. The results reveal an overall accuracy of 64.5% when only the post-event SAR image was used and an overall accuracy of 62.2% when the multi-temporal SAR images were used. We also used the building damage ratio (BDR) to evaluate performance. Damage ratios of 29.7%

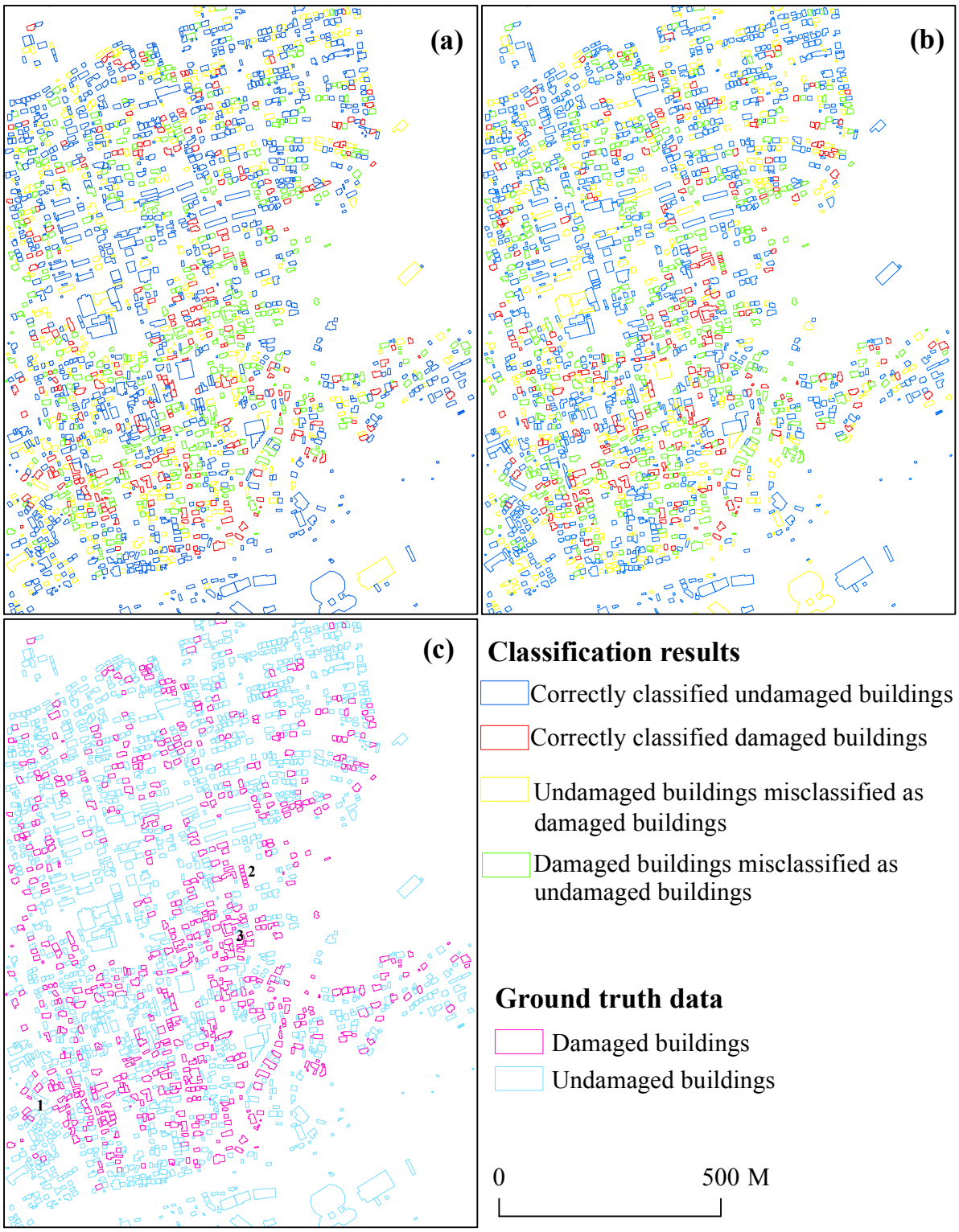

Fig. 5. Results of building damage classification using the K-Nearest Neighbors classifier: (a) damage mapping result using only the post-event SAR image; (b) damage mapping result using multi-temporal SAR images; (c) ground truth data in our study area. Note: numbers 1, 2 and 3 in **Figs. 5(c)** represent the positions of buildings in **Figs. 6(a)**, **6(b)** and **6(c)**, respectively.

and 31.3% were obtained for the control group and experimental group, respectively, both of which are quite close to the BDR of 29.1% obtained from the optical image of this area. Although the lower overall accuracy in this study cannot be used for detailed damage assessment, this high BDR accuracy can be used to determine the damage situation in certain disaster areas.

To grasp the factors underlying misclassification, post-

Table 3. Confusion matrix of building damage classification using the K-Nearest Neighbors classifier.

		Only post-event image			Multi-temporal image		
		Undamaged	Damaged	P.A.(%)	Undamaged	Damaged	P.A.(%)
GTD	Undamaged	1193	407	74.6%	1149	451	71.8%
	Damaged	393	263	40.1%	401	255	38.9%
	U.A.(%)	75.2%	39.2%		74.1%	36.1%	
		Overall accuracy=64.5% BDR=29.7%			Overall accuracy=62.2% BDR=31.3%		

Fig. 6. Three examples of building damage patterns that caused misclassification: (a) oblique building; (b) vertical sinking building; and (c) building with tile damage.

event high resolution satellite images [24] were employed for deep analysis. This consolidated three points of understanding as follow.

(1) Analysis of the reason that undamaged buildings are misclassified as damaged buildings

In this study, 407 undamaged buildings were misclassified as damaged buildings. **Fig. 6(a)** shows an example of an undamaged building that was misclassified as damaged; this building has relatively bigger azimuths between the side walls and the radar sensor's ground range direction (this building was referred to as oblique building) [34]. This is a typical case of overestimation. We can also confirm the radar azimuth direction in **Fig. 1(e)** and the building sidewall direction in **Fig. 5(c)**, which show that many buildings in our study area are oblique buildings. The building oblique buildings are represented as volume scattering [35]. Most of the randomly distributed damaged buildings are also represented by volume scattering [15]. The oblique buildings thus lead to their classification as damaged buildings.

(2) Analysis of the reasons damaged buildings are misclassified as undamaged buildings

An example of one damage pattern causing underestimation of damage is shown in **Fig. 6(b)**. This figure shows a vertical sinking building. Even though this building is severely damaged, the structure can still generate a strong double bounce reflection due to the relatively intact dihedral structure. This building will thus not show significant abnormality in scattering characteristics compared to surrounding buildings.

(3) Error analysis for buildings with damaged roof tiles

To achieve a convincing conclusion, it is best to carry out a control experiment. In order to clarify the impact of the degree of tile damage on classification, four adjacent buildings with similar geometry and azimuths, as shown in **Fig. 6(c)**, were selected for analysis. The upper two buildings with minor tile damage were misclassified as undamaged buildings, while the lower two buildings with significant tile damage were correctly classified as damaged buildings. This may indicate that having a large number of damaged tiles is more likely to cause higher heterogeneity of backscattering within the roof area, and therefore such buildings are easily classified as damaged. The undulating terrain is another important reason for the low classification accuracy. According to the field survey report, the northern part of the study area is located on a mountain slope where there is significant topographic relief, causing a change in the circular polarization correlation coefficient. This in turn causes extensive misclassification in the northern buildings. In such complex situations, it is quite difficult to distinguish this kind of damage from the undamaged buildings.

5. Conclusion

The mission of disaster science research is to develop the best strategies to minimize disaster losses. Faced with increasingly frequent and rampant natural disasters, we must improve our resilience to disasters. Synthetic Aperture Radar remote sensing is a useful tool for near real-time earthquake-induced building damage mapping. However, the wide variety of SAR image-based damage mapping methods may cause confusion about the choice of strategy when faced with an emergency disaster. In this research, a study was designed to quantitatively compare the performance of building damage mapping using only the post-event SAR image and mapping using multi-temporal SAR images in the framework of machine learning. The results reveal that the overall accuracy of building damage mapping when only the post-event SAR image was used is 64.5%, which is higher than the overall accuracy of 62.2% when both pre- and post-event SAR images were used. This result implies that the pre-event SAR image is not necessary for generating a reliable result. This study, however, is mainly a preliminary comparative study of SAR image-based damage mapping methods. More case study analysis is needed to consolidate or validate this idea. A limitation of our approach is that we only tested the distinguishability between undamaged and damaged buildings (totally collapsed, severely damaged and roof-damaged). Due to the limitations of SAR image resolution at present as well as to the specific imaging method of the radar sensor, it is quite difficult to distinguish severely damaged buildings and roof-damaged buildings from undamaged buildings. Different criteria for building damage categorization will be used to explore the potential of SAR images for building damage level classification in future work.

Acknowledgements

We would like to thank the Japan Aerospace Exploration Agency (JAXA) for providing the SAR imagery dataset. This work was supported by the JST CREST Project (Grant Number JPMJCR1411) and China Scholarship Council (CSC).

References:

[1] S.-H. Yun, K. Hudnut, S. Owen, F. Webb, M. Simons, P. Sacco, E. Gurrola, G. Manipon, C. Liang, E. Fielding, P. Milillo, H. Hua, and A. Coletta, "Rapid Damage Mapping for the 2015 M w 7.8 Gorkha Earthquake Using Synthetic Aperture Radar Data from COSMO-SkyMed and ALOS-2 Satellites," Seismological Research Letters, Vol.86, No.6, pp. 1549-1556, 2015.

[2] A. O. F. Geophysics, F. Track, and I. Nazionale, "A multisensor approach for the 2016 Amatrice earthquake damage assessment," No.1981, pp. 1-6, 2016.

[3] L. Ge, A. H.-M. Ng, X. Li, Y. Liu, Z. Du, and Q. Liu, "Near real-time satellite mapping of the 2015 Gorkha earthquake, Nepal," Annals of GIS, Vol.21, No.3, pp. 175-190, 2015.

[4] T. Balz and M. S. Liao, "Building-damage detection using postseismic high-resolution SAR satellite data," Int. J. of Remote Sensing, Vol.31, No.13, pp. 3369-3391, 2010.

[5] M. Matsuoka and F. Yamazaki, "Characteristics of satellite SAR images in the areas damaged by earthquakes," Int. Geoscience and Remote Sensing Symposium (IGARSS), Vol.6, pp. 2693-2696, 2000.

[6] M. Matsuoka and F. Yamazaki, "Building damage detection using satellite SAR intensity images for the 2003 Algeria and Iran earthquakes," Geoscience and Remote Sensing Symposium, Vol.2, pp. 1099-1102, 2004.

[7] M. Matsuoka and F. Yamazaki, "Building damage detection using SAR intensity images for recent earthquakes," European Space Agency, (Special Publication) ESA SP, No.572, pp. 2021-2026, 2005.

[8] M. Matsuoka and M. Estrada, "Development of earthquake-induced building damage estimation model based on ALOS/PALSAR observing the 2007 Peru earthquake," J. of Disaster Research, Vol.8, No.2, pp. 346–355, 2013.

[9] W. Liu, F. Yamazaki, and T. Sasagawa, "Monitoring of the Recovery Process of the Fukushima Daiichi Nuclear Power Plant from VHR SAR Images," Vol.11, No.2, 2016.

[10] F. Yamazaki, Y. Iwasaki, W. Liu, T. Nonaka, and T. Sasagawa, "Detection of damage to building side-walls in the 2011 Tohoku, Japan earthquake using high-resolution TerraSAR-X images," Vol.8892, pp. 1-9, 2013.

[11] S. Plank, "Rapid damage assessment by means of multi-temporal SAR-A comprehensive review and outlook to Sentinel-1," Remote Sensing, Vol.6, pp. 4870-4906, 2014.

[12] H. Miura, S. Midorikawa, and M. Matsuoka, "Building Damage Assessment Using High-Resolution Satellite SAR Images of the 2010 Haiti Earthquake," Earthquake Spectra, Vol.32, No.1, pp. 591-610, 2015.

[13] L. Dong and J. Shan, "A comprehensive review of earthquake-induced building damage detection with remote sensing techniques," ISPRS J. of Photogrammetry and Remote Sensing, Vol.84, pp. 85-99, 2013.

[14] R. Guida, A. Iodice, and D. Riccio, "Monitoring of collapsed builtup areas with high resolution SAR images," Geoscience and Remote Sensing Symposium (IGARSS), 2010 IEEE Int., pp. 2422-2425, 2010.

[15] S.-w. Chen, S. Member, and M. Sato, "Tsunami Damage Investigation of Built-Up Areas Using Multi-temporal Spaceborne Full Polarimetric SAR Images," Vol.51, No.4, pp. 1985-1997, 2013.

[16] J. Hoffmann, "Mapping damage during the Bam (Iran) earthquake using interferometric coherence," Int. J. of Remote Sensing, Vol.28, No.6, pp. 1199-1216, 2007.

[17] G. A. Arciniegas, W. Bijker, N. Kerle, and V. A. Tolpekin, "Coherence- and amplitude-based analysis of seismogenic damage in Bam, Iran, using ENVISAT ASAR data," IEEE Trans. on Geoscience and Remote Sensing, Vol.45, No.6, pp. 1571-1581, 2007.

[18] M. Watanabe, R. B. Thapa, T. Ohsumi, H. Fujiwara, C. Yonezawa, N. Tomii, and S. Suzuki, "Detection of damaged urban areas using interferometric SAR coherence change with PALSAR-2," Earth, Planets and Space, Vol.68, No.1, p. 131, 2016.

[19] W. Zhai and C. Huang, "Fast building damage mapping using a single post-earthquake PolSAR image: a case study of the 2010 Yushu earthquake," Earth, Planets and Space, Vol.68, No.1, p. 86, 2016.

[20] X. Li, H. Guo, L. Zhang, X. Chen, and L. Liang, "A New Approach to Collapsed Building Extraction Using RADARSAT-2 Polarimetric SAR Imagery," Vol.9, No.4, pp. 677-681, 2012.

[21] L. Shi, W. Sun, J. Yang, P. Li, and L. Lu, "Building Collapse Assessment by the Use of Postearthquake Chinese VHR Airborne SAR," IEEE Geoscience and Remote Sensing Letters, Vol.12, No.10, pp. 2021-2025, 2015.

[22] L. Gong, C. Wang, F. Wu, J. Zhang, H. Zhang, and Q. Li, "Earthquake-Induced Building Damage Detection with Post-Event Sub-Meter VHR TerraSAR-X Staring Spotlight Imagery," Remote Sensing, Vol.8, No.12, p. 887, 2016.

[23] Y. Hata, H. Goto, and M. Yoshimi, "Preliminary Analysis of Strong Ground Motions in the Heavily Damaged Zone in Mashiki Town, Kumamoto, Japan, during the Mainshock of the 2016 Kumamoto Earthquake (Mw7.0) Observed by a Dense Seismic Array," Seismological Research Letters, Vol.87, No.5, pp. 1044-1049, 2016.

[24] Map data Imagery@ Google, 2016, https://www.google.co.jp/maps [accessed December 1,2016]

[25] F. Dell'Acqua, C. Bignami, M. Chini, G. Lisini, D. A. Polli, and S. Stramondo, "Earthquake damages rapid mapping by satellite remote sensing data: L'Aquila april 6th, 2009 event," IEEE J. of Selected Topics in Applied Earth Observations and Remote Sensing, Vol.4, No.4, pp. 935-943, 2011.

[26] M. Hall, E. Frank, G. Holmes, B. Pfahringer, P. Reutemann, and I. H. Witten, "The WEKA data mining software," ACM SIGKDD Explorations Newsletter, Vol.11, No.1, p. 10, 2009.

[27] ENVI/SARscape, http://sarmap.ch/tutorials/Basic.pdf [accessed May 1, 2016]

[28] Sentinel Toolboxes, 2016, https://sentinel.esa.int/web/sentinel/toolboxes [accessed May 12, 2016]

[29] A. B. Owen, "Infinitely Imbalanced Logistic Regression," J. of Machine Learning Research, No.1, pp. 1-13, 2006.

[30] H. He and E. Garcia, "Learning from Imbalanced Data Sets.," IEEE Trans. on knowledge and data engineering, Vol.21, No.9, pp. 1263-1264, 2010.
[31] L. Zeng, "Logistic Regression in Rare Events Data," Political Analysis Vol.9, Issue 2, pp. 137-163, 2016.
[32] R. Blagus and L. Lusa, "Class prediction for high-dimensional class-imbalanced data," BMC Bioinformatics, Vol.11, No.1, p. 523, 2010.
[33] J. Burez and D. Van den Poel, "Handling class imbalance in customer churn prediction," Expert Systems with Applications, Vol.36, No.3 PART 1, pp. 4626-4636, 2009.
[34] M. Kajimoto and J. Susaki, "Urban Density Estimation From Polarimetric SAR Images Based on a POA Correction Method," IEEE Journal of Selected Topics in Applied Earth Observations and Remote Sensing, Vol.6, Issue: 3, pp. 1418-1429, 2013.
[35] Y. Yamaguchi, "Four-component scattering power decomposition using coherency matrix," Int. Geoscience and Remote Sensing Symposium (IGARSS), Vol.49, No.6, pp. 1044-1047, 2011.
[36] Y. Bai, B. Adriano, E. Mas, H. Gokon, and S. Koshimura, "Object-Based Building Damage Assessment Methodology Using Only Post Event ALOS-2/PALSAR-2 Dual Polarimetric SAR Intensity Images," J. of Disaster Research, Vol.12, No.2, p. 259, 2017.
[37] R. M. Haralick and K. Shanmugam, "Textural features for image classification," IEEE Trans. on systems, Man, and Cybernetics, Vol.SMC-3, Issue 6, pp. 610-621, 1973.
[38] A. B. Girisha, M. C. Chandrashekhar, and D. M. Kurian, "FPGA implementation of GLCM," Int. J. of Advanced Research in Electrical, Electronics and Instrumentation Engineering, Vol.2, Issue 6, 2013.

Name:
Yanbing Bai

Affiliation:
Ph.D. Student, Graduate School of Engineering, Tohoku University

Address:
Aoba 468-1, Aramaki, Aoba-ku, Sendai, 980-0845, Japan

Brief Career:
2011-2014 Master of Science, School of Earth and Space Sciences, Peking University, China
2014- PhD student, Graduate School of Engineering, Tohoku University, Japan
Jan. 2017-May 2017 Visiting Scholar, Bren School of Information and Computer Sciences, University of California, Irvine

Selected Publications:
• Y. Bai, B. Adriano, E. Mas, H. Gokon, and S. Koshimura, "Object-Based Building Damage Assessment Methodology Using Only Post Event ALOS-2/PALSAR-2 Dual Polarimetric SAR Intensity Images," Journal of Disaster Research, Vol.12, No.2, p.259, 2017.
• N. Wang, Q. Qin, L. Chen, and Y. Bai, "Dynamic monitoring of coalbed methane reservoirs using Super-Low Frequency electromagnetic prospecting," International Journal of Coal Geology, Vol.127, pp. 24-41, 2014.
• Y. Bai, B. Adriano, E. Mas, and S. Koshimura, "Developing a methodology for building damage mapping using only post-event dual-polarimetric SAR data – Case study from the 2015 Nepal earthquake. In the 2016 Asia Oceania Geosciences Society conference, pages CD-ROM, 2016.

Academic Societies & Scientific Organizations:
• Japan Society of Civil Engineers (JSCE)
• Earthquake Engineering Research Institute (EERI)

Name:
Bruno Adriano

Affiliation:
Postdoctoral Researcher, International Research Institute of Disaster Science (IRIDeS), Tohoku University

Address:
Aoba 468-1, Aramaki, Aoba-ku, Sendai 980-8579, Japan

Brief Career:
2010-2012 Assistant Professor, National University of Engineering, Peru
2012-2013 Research Student, ReGiD, IRIDeS, Tohoku University, Japan
2013-2016 PhD Civil Engineering, Graduate School of Engineering, Tohoku University, Japan
2016- JSPS Fellow, IRIDeS, Tohoku University, Japan

Selected Publications:
• B. Adriano, S. Hayashi, H. Gokon, E. Mas, and S. Koshimura, "Understanding the Extreme Tsunami Inundation in Onagawa Town by the 2011 Tohoku Earthquake, Its Effects in Urban Structures and Coastal Facilities," Coastal Engineering Journal, JSCE, Vol.58, pp. 1640013, 2016.

Academic Societies & Scientific Organizations:
• Peruvian Engineering College
• Japan Society of Civil Engineers (JSCE)
• Japan Geoscience Union (JpGU)
• American Geoscience Union (AGU)
• Institute of Electrical and Electronics Engineers (IEEE)

Name:
Erick Mas

Affiliation:
Associate Professor, International Research Institute of Disaster Science (IRIDeS), Tohoku University

Address:
Aoba 468-1, Aramaki, Aoba-ku, Sendai 980-8579, Japan

Brief Career:
1999-2004 B.S. Civil Engineering, National University of Engineering, Peru
2006-2009 M.Sc. Disaster Risk Management, National University of Engineering, Peru
2009-2012 PhD Civil Engineering, Tsunami Engineering, Tohoku University, Japan
2012-2016 Assistant Professor, IRIDeS, Tohoku University, Japan
2016- Associate Professor, IRIDeS, Tohoku University, Japan

Selected Publications:
• E. Mas, B. Adriano, S. Koshimura, F. Imamura, H. Kuroiwa, F. Yamazaki, C. Zavala, and M. Estrada, "Identifying Evacuee's Demand of Tsunami Shelters using Agent Based Simulation. Published on Tsunami Events and Lessons Learned," Y. Kontar, V. Santiago-Fandino, T. Takahashi (Eds.), Springer Netherlands, 2014.
• E. Mas, A. Suppasri, F. Imamura, and S. Koshimura, "Agent Based simulation of the 2011 Great East Japan Earthquake Tsunami evacuation. An integrated model of tsunami inundation and evacuation," Journal of Natural Disaster Science, Vol.34, Issue 1, pp. 41-57, 2012.

Academic Societies & Scientific Organizations:
• Peruvian Engineering College (PEC)
• Japan Society of Civil Engineers (JSCE)
• Japan Geoscience Union (JpGU)
• European Geosciences Union (EGU)
• American Geophysical Union (AGU)

Name:
Shunichi Koshimura

Affiliation:
Professor, Laboratory of Remote Sensing and Geoinformatics for Disaster Management, International Research Institute of Disaster Science, Tohoku University

Address:
Aoba 6-6-03, Sendai 980-8579, Japan

Brief Career:
2002-2005 Research Scientist, Disaster Reduction and Human Renovation Institute, Japan
2005-2012 Associate Professor, Tohoku University, Japan
2012- Professor, ReGiD, IRIDeS, Tohoku University, Japan

Selected Publications:
• S. Koshimura, T. Oie, H. Yanagisawa, and F. Imamura, "Developing fragility functions for tsunami damage estimation using numerical model and post-tsunami data from Banda Aceh, Indonesia," Coastal Engineering Journal, No.3, pp. 243-273, 2009.
• S. Koshimura, Y. Hayashi, K. Munemoto, and F. Imamura, "Effect of the Emperor seamounts on trans-oceanic propagation of the 2006 Kuril Island earthquake tsunami," Geophysical Research letters, Vol.35, L02611, doi:10.1029/2007GL032129, 24, 2008.
• S. Koshimura, T. Katada, H. O. Mofjeld, and Y. Kawata, "A method for estimating casualties due to the tsunami inundation flow," Natural Hazards, Vol.39, pp. 265-274, 2006.

Academic Societies & Scientific Organizations:
• Japan Society of Civil Engineers (JSCE)
• Institute of Social Safety Science (ISSS)
• Japan Associaiton for Earthquake Engineering (JAEE)
• Japan Society for Computational Engineering and Science (JSCES)
• Americal Geophysical Union (AGU)